Rate constant and secondary organic aerosol formation from the gas-phase reaction of eugenol with hydroxyl radicals

Changgeng Liu[1,2], Yongchun Liu[3,*], Tianzeng Chen[1,5], Jun Liu[1,5], Hong He[1,4,5,*]

[1]State Key Joint Laboratory of Environment Simulation and Pollution Control, Research Center for Eco-Environmental Sciences, Chinese Academy of Sciences, Beijing 100085, China

[2]School of Biological and Chemical Engineering, Panzhihua University, Panzhihua 617000, China

[3]Beijing Advanced Innovation Center for Soft Matter Science and Engineering, Beijing University of Chemical Technology, Beijing 100029, China

[4]Center for Excellence in Regional Atmospheric Environment, Institute of Urban Environment, Chinese Academy of Sciences, Xiamen 361021, China

[5]University of Chinese Academy of Sciences, Beijing 100049, China

Correspondence to: Yongchun Liu (liuyc@buct.edu.cn) and Hong He (honghe@rcees.ac.cn)

Abstract. Methoxyphenols are an important organic component of wood-burning emissions and considered to be potential precursors of secondary organic aerosols (SOA). In this work, the rate constant and SOA formation potential for the OH-initiated reaction of 4-allyl-2-methoxyphenol (eugenol) were investigated for the first time in an oxidation flow reactor (OFR). The rate constant was $(8.01 \pm 0.40) \times 10^{-11}$ cm^3 molecule^{-1} s^{-1}, determined by the relative rate method. The SOA yield first increased and then decreased as a function of OH exposure, and was also dependent on eugenol concentration. The maximum SOA yields (0.11−0.31) obtained at different eugenol concentrations could be expressed well by a one-product model. The carbon oxidation state (OS_C) increased linearly and significantly as OH exposure rose, indicating that the high oxidation degree was achieved for SOA. In addition, the presence of SO_2 (0−198 ppbv) and NO_2 (0−109 ppbv) was conducive to increasing SOA yield, for which the maximum enhancement values were 38.6% and 19.2%, respectively. The N/C ratio (0.032−0.043) indicated that NO_2 participated in the OH-initiated reaction, subsequently forming organic nitrates. The results could be helpful for further understanding the SOA formation potential from the atmospheric oxidation of methoxyphenols and the atmospheric aging process of smoke plumes from biomass-burning emissions.

2

1 Introduction

Wood combustion is a major contributor to atmospheric fine particulate matter (PM) (Bruns et al., 2016), which could contribute approximately 10−50% of the total organic fraction of atmospheric aerosols (Schauer and Cass, 2000). In some regions with cold climates, wood smoke-associated aerosols are estimated to account for more than 70% of $PM_{2.5}$ in winter (Jeong et al., 2008; Ward et al., 2006). Recently, significant potential of secondary organic aerosol (SOA) formation from wood smoke emissions has been reported (Bruns et al., 2016; Gilardoni et al., 2016; Tiitta et al., 2016; Ciarelli et al., 2017; Ding et al., 2017). In addition, the organic compounds derived from wood combustion and their oxidation products may contribute significantly to global warming due to their light-absorbing properties (Chen and Bond, 2010). It has been reported that wood smoke particles are predominant in the inhalable size range (Bari et al., 2010) and their extracts are mutagenic (Kleindienst et al., 1986). Exposure to wood smoke can result in adverse health effects associated with acute respiratory infections, tuberculosis, lung cancer, cataracts, etc. (Bolling et al., 2009). Therefore, wood combustion has multifaceted impacts on climate, air quality, and human health.

Methoxyphenols produced by lignin pyrolysis are potential tracers for wood smoke, and their emission rates are in the range of 900−4200 mg kg^{-1} wood (Schauer et al., 2001; Simpson et al., 2005; Nolte et al., 2001). The highest level of methoxyphenols in the atmosphere always appears during a wood smoke-dominated period, with observed values up to several mg m^{-3} (Schauer and Cass, 2000; Schauer et al., 2001; Simpson et

al., 2005). Methoxyphenols are semi-volatile aromatic compounds with low molecular

weight, and many of them are found to mainly exist in the gas phase at typical ambient

temperature (Schauer et al., 2001; Simpson et al., 2005). Thus, methoxyphenols can be

chemically transformed through gas-phase reactions with atmospheric oxidants (Coeur-

Tourneur et al., 2010a; Lauraguais et al., 2012, 2014a, 2014b, 2015, 2016; Yang et al.,

2016; Zhang et al., 2016; El Zein et al., 2015). The corresponding rate constants control

their effectiveness as stable tracers for wood combustion and atmospheric lifetimes. In

recent years, the rate constants for the gas-phase reactions of some methoxyphenols

with hydroxyl (OH) radicals (Coeur-Tourneur et al., 2010a; Lauraguais et al., 2012,

2014b, 2015), nitrate (NO_3) radicals (Lauraguais et al., 2016; Yang et al., 2016; Zhang

et al., 2016), chlorine atoms (Cl) (Lauraguais et al., 2014a) and ozone (O_3) (El Zein et

al., 2015) have been determined. Some studies have indicated significant SOA

formation from 2,6-dimethoxyphenol (syringol) and 2-methoxyphenol (guaiacol) with

respect to their reactions with OH radicals (Sun et al., 2010; Lauraguais et al., 2012,

2014b; Ahmad et al., 2017; Yee et al., 2013; Ofner et al., 2011). Although biomass-

burning emissions have been indicated to have great SOA formation potential via

atmospheric oxidation (Bruns et al., 2016; Gilardoni et al., 2016; Li et al., 2017; Ciarelli

et al., 2017; Ding et al., 2017), SOA formation and growth from methoxyphenols are

still poorly understood. Besides, the observed SOA levels in the atmosphere cannot be

well explained by the present knowledge on SOA formation, which reflects the fact that

a large number of precursors are not taken into account in the SOA-formation reactions

76   included in the atmospheric models (Lauraguais et al., 2012).

77   4-Allyl-2-methoxyphenol (eugenol) is a typical methoxyphenol produced by ligin

78   pyrolysis with a branched alkene group. It is widely detected in the atmosphere with

79   the concentration on the order of ng m^{-3}, which is comparable to those of other

80   methoxyphenols (e.g., guaiacol and syringol) (Schauer et al., 2001; Simpson et al., 2005;

81   Bari et al., 2009). Its average emission concentration and factor in beech burning are

82   0.032 μg m^{-3} and 1.52 μg g^{-1} PM, respectively, which are both higher than those (0.016

83   μg m^{-3} and 0.762 μg g^{-1} PM) of guaiacol (Bari et al., 2009). It has even be detected in

84   human urine after exposure to wood smoke (Dills et al., 2006). Eugenol has been

85   observed to mainly distribute in the gas phase in wood smoke emissions (Schauer et al.,

86   2001), and its gas/particle-partition coefficient is lower than 0.01 (Zhang et al., 2016),

87   thus indicating the importance of its gas-phase reactions in the atmosphere. For this

88   reason, the aim of this work was to determine the rate constant and explore the SOA

89   formation potential for eugenol in the gas-phase reaction with OH radicals using an

90   Oxidation Flow Reactor (OFR). In addition, the effects of SO_2 and NO_2 on SOA

91   formation were investigated. To our knowledge, this work represents the first

92   determination of the rate constant and SOA yield for the gas-phase reaction of eugenol

93   with OH radicals.

94   **2   Experimental section**

95   The detailed schematic description of the experimental system used in this work is

96   shown in Figs. S1 and S2. The gas-phase reactions were conducted in the OFR, of which

97   detailed description has been presented elsewhere (Liu et al., 2014b). Before entering

98   into the OFR, gas-phase species were mixed thoroughly in the mixing tube. The

99   reaction time in the OFR was 26.7 s, calculated according to the illuminated volume

100   (0.89 L) and the total flow rate (2 L min^{-1}). OH radicals were generated by photolysis

101   of O_3 in the presence of water vapor using a 254 nm UV lamp (Jelight Co., Inc.), and

102   their formation reactions have been described elsewhere (Zhang et al., 2017). The

103   concentration of OH radicals was governed by O_3 concentration and relative humidity

104   (RH). O_3 concentration was controlled by changing the unshaded length of a 185 nm

105   UV lamp (Jelight Co., Inc.). O_3 with the concentration of 0.94−9.11 ppmv in the OFR

106   was produced by passing zero air through an O_3 generator (Model 610-220, Jelight Co.,

107   Inc.), which was used to produce OH radicals. RH and temperature in the OFR were

108   (44.0 ± 2.0)% and (301 ± 1) K, respectively, measured at the outlet of the OFR. The

109   steady-state concentrations of OH radicals were determined using SO_2 as the reference

110   compound in separate calibration experiments. It is a widely-used method for

111   calculating OH exposure in the OFR, but could not well describe the potential OH

112   suppression caused by the added external OH reactivity (Zhang et al., 2017; Lambe et

113   al., 2015; Simonen et al., 2017; Li et al., 2015; Peng et al., 2015, 2016). The decay of

114   SO_2 from its reaction with OH radicals (9×10^{-13} cm^3 molecule^{-1} s^{-1}) (Davis et al., 1979)

115   was measured by a SO_2 analyzer (Model 43i, Thermo Fisher Scientific Inc.). The

116   concentration of OH radicals ([OH]) in this work ranged from approximately 4.5×10^9

117   to 4.7×10^{10} molecules cm^{-3}, and the corresponding OH exposures were in the range of

118　1.21−12.55 × 10^{11} molecules cm^{-3} s or approximately 0.93 to 9.68 d of equivalent

119　atmospheric exposure, which was calculated using a typical [OH] of 1.5 × 10^6

120　molecules cm^{-3} in the atmosphere (Mao et al., 2009).

121　　　An Aerodyne high-resolution time-of-flight aerosol mass spectrometer (HR-ToF-

122　AMS) was applied to perform online measurement of the chemical composition of

123　particles and the non-refractory submicron aerosol mass (DeCarlo et al., 2006). The

124　size distribution and concentration of particles were monitored by a scanning mobility

125　particle sizer (SMPS), consisting of a differential mobility analyzer (DMA) (Model

126　3082, TSI Inc.) and a condensation particle counter (CPC) (Model 3776, TSI Inc.).

127　Assuming that particles are spherical and non-porous, the average effective particle

128　density could be calculated to be 1.5 g cm^{-3} using the equation $\rho=d_{va}/d_m$ (DeCarlo et al.,

129　2004), where d_{va} is the mean vacuum aerodynamic diameter measured by the HR-ToF-

130　AMS and d_m is the mean volume-weighted mobility diameter measured by the SMPS.

131　The particle size for HR-ToF-AMS measurement was calibrated using NH$_4$NO$_3$

132　particles with the diameter between 60−700 nm selected by a DMA. The mass

133　concentration of particles measured by HR-ToF-AMS was corrected by SMPS data in

134　this work using the same method as Gordon et al. (2014). Eugenol and reference

135　compounds were measured by a high-resolution proton-transfer reaction time-of-flight

136　mass spectrometer (HR-ToF-PTRMS) (Ionicon Analytik GmbH). More experimental

137　details were described in the Supplement.

138　**3　Results and discussion**

3.1 Rate constant

The possible effect of O_3 on the decay of eugenol and reference compounds was investigated in this work. As shown in Fig. S3, their concentrations were not affected by O_3. Meanwhile, no SOA formation was observed by the SMPS and HR-ToF-AMS. In addition, in order to investigate the possible photolysis of eugenol and reference compounds at 254 nm UV light in the OFR, the comparative experiments were conducted with UV lamp turned on and turned off, when eugenol and reference compounds were introduced into the OFR. The normalized mass spectra of eugenol and reference compounds in the dark and light were shown in Fig. S4. The results showed that no significant decay (< 5%) by photolysis was observed and could be neglected. According to the results reported by Peng et al. (2016), the photolysis of phenol and 1,3,5-trimethylbenzene could be ignored when the ratio of exposure to 254 nm and OH is lower than 1×10^6 cm s^{-1}, of which values (1.6×10^2 to 1.7×10^3 cm s^{-1}) in this work also met this condition. In addition, the initial concentration of eugenol was determined with UV lamp turned on. Therefore, the effect of photolysis could be neglected in this work. However, it cannot be ruled out that photolysis under UV irradiation might have influence on the evolution of the oxidation products.

The rate constant for the gas-phase reaction of eugenol with OH radicals was determined by the relative rate method, which can be expressed as the following equation (Coeur-Tourneur et al., 2010a; Yang et al., 2016; Zhang et al., 2016):

$$\ln(C_{E0}/C_{Et}) = \ln(C_{R0}/C_{Rt})k_E / k_R \tag{1}$$

160   where C_{E0} and C_{Et} are the initial and real-time concentrations of eugenol, respectively.

161   k_E is the rate constant of the eugenol reaction with OH radicals. C_{R0} and C_{Rt} are the

162   initial and real-time concentrations of reference compound, respectively. k_R is the rate

163   constant of the reference compound with OH radicals, of which values for m-xylene

164   and 1,3,5-trimethylbenzene are 2.20×10^{-11} and 5.67×10^{-11} cm^3 molecule^{-1} s^{-1},

165   respectively (Kramp and Paulson, 1998; Coeur-Tourneur et al., 2010a).

166   Data obtained from the reactions were plotted in the form of Eq. (1) and were well

167   fitted by linear regression ($R^2 > 0.97$, Fig. 1). A summary of the slopes and the rate

168   constants are listed in Table 1. The errors in k_E/k_R are the standard deviations generated

169   from the linear regression analysis and do not include the uncertainty in the rate

170   constants of the reference compounds. The rate constants are $(7.54 \pm 0.28) \times 10^{-11}$ and

171     $(8.47 \pm 0.51) \times 10^{-11}$ cm^3 molecule^{-1} s^{-1}, respectively, when using 1,3,5-

172   trimethylbenzene and m-xylene as reference compounds. According to the US EPA

173   AOP WIN model based on the structure activity relationship (SAR) (US EPA, 2012),

174   the rate constant was calculated to be 6.50×10^{-11} cm^3 molecule^{-1} s^{-1} (Table 1), which

175   is lower than that obtained in this work. Inaccurate performance of the AOP WIN model

176   has been observed for other multifunctional organics due to the inaccurate

177   representation of the eletronic effects of different functional groups on reactivity

178   (Coeur-Tourneur et al., 2010a; Lauraguais et al., 2012). In addition, the difference

179   between density functional theory (DFT) calculation and lab study has been also

180   observed. For example, the DFT-predicted rate constant of 2-methoxyphenol with OH

181 radicals (12.19×10^{-11} cm^3 molecule^{-1} s^{-1}) is higher than that (7.53×10^{-11} cm^3 molecule^{-1}

182 s^{-1}) obtained by lab study (Coeur-Tourneur et al., 2010a; Priya and Lakshmipathi,

183 2017). These suggest that it is necessary to determine the rate constants of

184 multifunctional organics through lab experiments. The rate constant determined in this

185 work can be used to calculate the atmospheric lifetime of eugenol with respect to its

186 reaction with OH radicals. Assuming a typical [OH] for a 24 h average value to be 1.5

187 $\times 10^6$ molecules cm^{-3} (Mao et al., 2009), the corresponding lifetime of eugenol was

188 calculated to be (2.31 ± 0.12) h with the average rate constant of (8.01 ± 0.40) $\times 10^{-11}$

189 cm^3 molecule^{-1} s^{-1}. This short lifetime indicates that eugenol is too reactive to be used

190 as a tracer for wood smoke emissions, and also implies the possible fast conversion of

191 eugenol from gas-phase to secondary aerosol during the transportation process.

192   The rate constant obtained in this work is about 2 orders of magnitude faster than

193 that for eugenol with NO$_3$ radicals (1.6×10^{-13} cm^3 molecule^{-1} s^{-1}) (Zhang et al., 2016),

194 which suggests that the OH-initiated reaction of eugenol might be the main chemical

195 transformation in the atmosphere. The rate constants of the OH-initiated reactions of

196 guaiacol, 2,6-dimethylphenol, and syringol were 7.53×10^{-11}, 6.70×10^{-11}, and $9.66 \times$

197 10^{-11} cm^3 molecule^{-1} s^{-1}, respectively (Coeur-Tourneur et al., 2010a; Thuner et al., 2004;

198 Lauraguais et al., 2012), while their corresponding rate constants were calculated to be

199 2.98×10^{-11}, 5.04×10^{-11}, and 16.51×10^{-11} cm^3 molecule^{-1} s^{-1}, according to the US EPA

200 AOP WIN model (US EPA, 2012). These differences among rate constants suggest that

201 the rate constants of multifunctional organics should be necessarily determined via lab

202 experiments. The reactivity of eugenol toward OH radicals is slightly higher than those

203 of guaiacol and 2,6-dimethylphenol, while slightly slower than that of syringol. The

204 presence of two methoxyl groups ($-OCH_3$) in syringol activates the electrophilic

205 addition of OH radicals to the benzene ring by donating electron density through the

206 resonance effect (Lauraguais et al., 2016). The activation effect of the methoxyl group

207 is much larger than those of alkyl groups (McMurry, 2004). In a recent study, the

208 reported energy barrier of NO_3 electrophilic addition to eugenol was about 2-fold than

209 that of 4-ethylguaiacol, indicating that the activation effect of the allyl group

210 ($-CH_2CH=CH_2$) is lower than that of the ethyl group ($-CH_2CH_3$) (Zhang et al., 2016).

211 These results are in accordance with the activation effects of the substituants toward the

212 electrophilic addition of OH radicals (McMurry, 2004).

213 **3.2   Effects of eugenol concentration and OH exposure on SOA formation**

214 In this work, a series of experiments were conducted in the OFR with different eugenol

215 concentrations. The SOA yield was determined as the ratio of the SOA mass

216 concentration (M_o μg m^{-3}) to the reacted eugenol concentration ($\triangle$[eugenol], μg m^{-3})

217 (Kang et al., 2007). The experimental conditions and maximum SOA yields are listed

218 in Table 2. The wall loss of aerosol particles in the OFR could be ignored, according to

219 our previous results reported by Liu et al. (2014a). Fig. S5 shows the plots of the SOA

220 yield versus OH exposure at different eugenol concentrations. Higher concentrations

221 resulted in higher amounts of condensable products and subsequently increased SOA

222 yield (Lauraguais et al., 2012). SOA mass also directly influences the gas/particle

223　　partitioning, because SOA can serve as the adsorption medium for oxidation products,

224　　and higher SOA mass generally results in higher SOA yield (Lauraguais et al., 2012,

225　　2014b). In the OFR, in all cases the SOA yield first increased and then decreased as a

226　　function of OH exposure (Fig. S5). This trend is the most common phenomenon

227　　observed in the studies conducted in the OFR and Potential Aerosol Mass (PAM) reactor

228　　(Lambe et al., 2015; Ortega et al., 2016; Palm et al., 2016, 2018; Simonen et al., 2017).

229　　In this work, according to the OFR exposure estimator (v2.3) developed by Jimenez's

230　　group based on the estimation equations reported in the previous work (Li et al., 2015;

231　　Peng et al., 2015, 2016), the maximum reduction of OH exposure by eugenol in the

232　　OFR was approximately 90%. Its detailed calculation has been shown in the

233　　Supplement. Although OH suppression by eugenol was not well determined in the OFR,

234　　OH radicals were expected to be the main oxidant due to the fast reaction rate constant

235　　of eugenol toward OH radicals obtained in this work. The decrease of SOA yield at high

236　　OH exposure is possibly contributed from the C−C bond scission of gas-phase species

237　　by further oxidation or heterogeneous reactions involving OH radicals, which would

238　　generate a large amount of fragmented molecules that subsequently volatilize out of

239　　aerosol particles (Lambe et al., 2015; Ortega et al., 2016; Simonen et al., 2017).

240　　　　SOA yield can be described using a widely-used semi-empirical model on the basis

241　　of the absorptive gas-particle partitioning of semi-volatile products, in which the overall

242　　SOA yield (Y) is given by (Odum et al., 1996):

243　　$Y = \sum_i M_o \frac{\alpha_i K_{om,i}}{1 + K_{om,i} M_o}$ （2）

244   where α_i is the mass-based stoichiometric coefficient for the reaction producing the

245   semi-volatile product i, $K_{om,i}$ is the gas-particle partitioning equilibrium constant, and

246   M_o is the total aerosol mass concentration.

247   The SOA yield data in Table 2 can be plotted in the form of Eq. (2) to obtain the

248   yield curve for eugenol (Fig. 2). The simulation of experimental data indicated that a

249   one-product model could accurately reproduce the data ($R^2 = 0.98$), while the use of

250   two or more products in the model did not significantly improve the fitting quality.

251   Odum et al. (1996) reported that the SOA yield data from the oxidation of aromatic

252   compounds could be fitted well using a two-product model. However, a one-product

253   model was also efficient for describing the SOA yields from the oxidation of aromatics

254   including methoxyphenols (Coeur-Tourneur et al., 2010b; Lauraguais et al., 2012,

255   2014b). The success of simulation with a one-product model in this work is likely to

256   indicate that the products in SOA have similar values of α_i and $K_{om,i}$, i.e., that the

257   obtained α_i (0.36 ± 0.02) and $K_{om,i}$ ($0.013 \pm 0.002 \ m^3 \ ug^{-1}$) represent the average values.

258   In this work, considering that the product composition of SOA was not determined, the

259   volatility basis set (VBS) approach was not applied to simulate SOA yields. Fig. S6

260   shows a plot of the SOA mass concentration (M_o) versus the reacted eugenol

261   concentration ($\triangle$[eugenol]). Its slope was 0.37 as obtained using linear least-squares

262   fitting, which is very close to the α_i value (0.36). This suggests that the low-volatility

263   products formed in the reaction almost completely disperse on the particle phase

264   according to the theoretical partition model (Lauraguais et al., 2012, 2014b). In other

265 words, SOA yield was approximately an upper limit for eugenol oxidation in the OFR.

266 In view of the residence time in this work, it seems be in contradiction with the

267 recommendation of longer residence time made by Ahlberg et al. (2017), who found

268 that the condensation of low-volatility species on SOA in the OFR was often kinetically

269 limited at low mass concentrations. In our recent experiments (not published), the SOA

270 yields for guaiacol oxidation by OH radicals obtained under the similar experimental

271 conditions as this work, could be comparable to those obtained in the chamber studies

272 conducted at low RH (Fig. S7) (Lauraguais et al., 2014b;Yee et al., 2013). This suggests

273 that the effect of kinetic limitations on SOA condensation for the OH-initiated oxidation

274 of methoxyphenols in this system might be not important.

275   Elemental ratios (H/C and O/C) could provide insights into SOA composition and

276 chemical processes along with aging (Bruns et al., 2015). As shown in Fig. 3, O/C ratio

277 of SOA increased and H/C ratio decreased with increasing OH exposure, because

278 oxygen-containing functional groups were formed in the oxidation products. In addition,

279 the organic mass fractions of m/z 44 (CO_2^+) and m/z 43 (mostly $C_2H_3O^+$), named f_{44}

280 and f_{43}, respectively, could also provide information about the nature of SOA formation.

281 Fig. S8 shows the evolution of f_{44} and f_{43} versus OH exposure at low (272 μg m^{-3}) and

282 high (1328 μg m^{-3}) concentrations of eugenol. The values of f_{44} were much higher than

283 those of f_{43}, and increased significantly as a function of OH exposure, suggesting that

284 SOA formed in the experiments became more oxidized. The f_{44} value in this work

285 ranged up to 0.26, which was consistent with that observed for ambient low-volatility

286   (LV-OA), higher than 0.25 (Ng et al., 2010).

287   The average carbon oxidation state (OS_C) proposed by Kroll et al. (2011) is

288   considered a more accurate indicator of the oxidation degree of atmospheric organic

289   species than the O/C ratio alone, because it takes into account the saturation level of the

290   carbon atoms in the SOA. OS_C is defined as $OS_C = 2O/C - H/C$ (Kroll et al., 2011),

291   calculated according to the elemental composition of SOA measured by the HR-ToF-

292   AMS. In this work, the OS_C values obtained at low (272 μg m^{-3}) and high (1328 μg m^{-}

293   ^{3}) concentrations of eugenol were compared. As shown in Fig. 3, OS_C values for low

294   concentration (0.035−1.78) were much larger than those for high concentration

295   (0.0036−1.09), and increased linearly ($R^2 > 0.96$) with OH exposure of (1.21−12.55) ×

296   10^{11} molecules cm^{-3} s. The results were well supported by the evolution of SOA mass

297   spectra obtained by the HR-ToF-AMS at the same eugenol concentrations (Fig. S9).

298   Similar trends have been observed in the smog chamber and PAM reactor (Simonen et

299   al., 2017; Ortega et al., 2016). The OS_C value in this work extended as high as 1.78,

300   which was in good agreement with that observed for ambient LV-OA, up to 1.9 (Kroll

301   et al., 2011). Recently, Ortega et al. (2016) reported that the OS_C value for SOA formed

302   from ambient air in an OFR ranged up to 2.0; and Simonen et al. (2017) determined a

303   high OS_C value (> 1.1) for SOA formed from the OH-initiated reaction of toluene in a

304   PAM reactor with an OH exposure of 1.2×10^{12} molecules cm^{-3} s. In general, the OS_C

305   values for the PAM reactor are higher than those for smog chambers because OH

306   exposure in the PAM reactor is about 1−3 orders of magnitude higher than that in smog

307   chamber (Simonen et al., 2017; Ortega et al., 2016; Lambe et al., 2015). Higher OS_C

308   value indicates greater age, where the SOA components are further oxidized through

309   heterogeneous oxidation, adding substantial oxygen and reducing hydrogen in the

310   molecules in the particle-phase to increase OS_C values despite the overall loss of SOA

311   mass (Ortega et al., 2016).

312   **3.3   Effect of SO_2 on SOA formation**

313   As shown in Fig. 4, the presence of SO_2 favored SOA formation, and the sulfate

314   concentration increased linearly (R^2 = 0.99) as a function of OH exposure. The

315   maximum SOA yield enhancement of 38.6% was obtained at OH exposure of 5.41 ×

316   10^{11} molecules cm^{-3} s, and then decreased with the increase of OH exposure possibly

317   due to the fragmented molecules formed through the oxidation of gas-phase species by

318   high OH exposure (Lambe et al., 2015; Ortega et al., 2016; Simonen et al., 2017). The

319   SOA yield and sulfate concentration both increased linearly (R^2 > 0.97) as SO_2

320   concentration increased from 0 to 198 ppbv at OH exposure of 1.21 × 10^{11} molecules

321   cm^{-3} s (Fig. S10). Compared to the initial SOA yield (0.049) obtained in the absence of

322   SO_2, the SOA yield (0.066) obtained in the presence of 198 ppbv SO_2 was enhanced by

323   34.7%. In previous studies, Kleindienst et al. (2006) reported that the SOA yield from

324   α-pinene photooxidation increased by 40% in the presence of 252 ppbv SO_2; Liu et al.

325   (2016b) recently found that the SOA yield from 5 h photochemical aging of gasoline

326   vehicle exhaust was enhanced by 60−200% in the presence of ~150 ppbv SO_2.

327   As shown in Figs. 4 and S10, the increase of sulfate concentration was favorable

328 for SOA formation. In this system, it is difficult to completely remove trace NH_3, thus

329 the formed sulfate was the mixture of sulfuric acid (H_2SO_4) and a small amounts of

330 ammonium sulfate ((NH_4)$_2SO_4$). The in situ particle acidity was calculated as the H^+

331 concentration ([H^+], 40.23−648.39 nmol m^{-3}) according to the AIM-II model for the

332 $H^+ - NH_4^+ - SO_4^{2-} - NO_3^- - H_2O$ systems (http://www.aim.env.uea.ac.uk/aim/model2

333 /model2a.php; Liu et al., 2016b). The detailed description of the calculation method has

334 been represented elsewhere (Liu et al., 2016b). The elevated concentration of sulfate in

335 the particle phase with the increases of SO_2 concentration and OH exposure was an

336 important reason for the enhanced SOA yields (Kleindienst et al., 2006; Liu et al.,

337 2016b). Cao and Jang (2007) indicated that SOA yields from the oxidation of toluene

338 and 1,3,5-trimethylbenzene increased by 14−36% in the presence of acid seeds, with

339 [H^+] of 240−860 nmol m^{-3} compared to those obtained in the presence of nonacid seeds.

340 Similar results concerning the effect of particle acidity on SOA yields were reported in

341 other studies (Kleindienst et al., 2006; Liu et al., 2016b; Jaoui et al., 2008; Xu et al.,

342 2016). However, Ng et al. (2007b) found that particle acidity had a negligible effect on

343 SOA yields from photooxidation of aromatics, possibly due to the low RH (~5%) used

344 in their work. The water content of aerosol plays an essential role in acidity effects (Cao

345 and Jang, 2007). Under acidic conditions, the gas-phase oxidation products of eugenol

346 partitioned onto the particle-phase would be further oxidized into low volatility

347 products or produce oligomers by acid-catalyzed heterogeneous reactions, subsequently

348 enhancing SOA yields (Cao and Jang, 2007; Jaoui et al., 2008; Liu et al., 2016b; Xu et

349　al., 2016). In addition, the formed sulfate not only serves as the substrate for product

350　condensation and likely participates in new particle formation (NPF) (Jaoui et al., 2008;

351　Wang et al., 2016), but also enhances the surface areas of particles to facilitate

352　heterogeneous reactions on aerosols (Xu et al., 2016). These roles of sulfate are also

353　favorable for increasing SOA yields. Recently, Friedman et al. (2016) have indicated

354　that SO_2 could participate in the oxidation reactions of α-and β-pinene and perturbs

355　their oxidation in the OFR, but this possible effect could be ignored in this work due to

356　the relatively high RH and the negligible S/C ratio observed by the HR-ToF-AMS

357　(Friedman et al., 2016).

358　**3.4　Effect of NO_2 on SOA formation**

359　It is well known that high NO_x concentration almost always plays a negative role in

360　NPF and SOA formation because the reaction of NO with RO_2 radicals would result in

361　the formation of more volatile products compared to the reaction of HO_2 with RO_2

362　radicals (Sarrafzadeh et al., 2016). Previous studies reported that nitro-substituted

363　products were the main products for SOA formed from OH-initiated reactions of phenol

364　precursors including methoxyphenols, in the presence of NO_x (Ahmad et al., 2017;

365　Finewax et al., 2018; Lauraguais et al., 2012, 2014b). Thus, the effect of NO_2 on SOA

366　formation from eugenol oxidation by OH radicals was investigated. As shown in Fig.

367　5, the nitrate concentration measured by the HR-ToF-AMS increased as a function of

368　OH exposure in the presence of 40 ppbv NO_2, but it was much lower than the sulfate

369　concentration (Fig. 4) even though the OH rate constant for NO_2 was faster than that

370   for SO_2 (Atkinson et al., 1976; Davis et al., 1979). The possible explanation was that

371   the formed HNO_3 mainly existed in the gas phase, and the relatively high temperature

372    $(301 \pm 1$ K) was not favorable for gaseous HNO_3 distribution in the particle phase

373   (Wang et al., 2016). It has been indicated that the temperature range for the greatest loss

374   of nitrate is 293−298 K (Keck and Wittmaack, 2005). As illustrated in Fig. 5, the SOA

375   yield enhancement and N/C ratio both increased firstly and then decreased with rising

376   OH exposure. The increase of NO_2 concentration (40−109 ppbv) was beneficial to SOA

377   yields (0.053−0.062), N/C ratio (0.032−0.041), and nitrate formation (4.29−6.30 μg m^{-}

378   ^{3}) (Fig. S11). Compared to the presence of 41 ppbv SO_2, the maximum SOA yield

379   enhancement (19.17%) in the presence of 40 ppbv NO_2 was lower. For most aromatic

380   precursors, the addition of ppbv levels of NO_2 should have a negligible effect on SOA

381   formation, because the rate constants of phenoxy radicals with O_2 and NO_2 are on the

382   order of approximate 10^{-16} and 10^{-11} cm^3 molecule^{-1} s^{-1}, respectively (Atkinson and Arey,

383   2003). But, for phenol precursors only about 0.5 ppbv NO_2 is enough to compete with

384   O_2 for the reaction with phenoxy radicals (Finewax et al., 2018). Therefore, the

385   enhancement effect of NO_2 on SOA formation might be relevant to the special case of

386   phenols or methoxyphenols but not for other aromatic precursors.

387   It is noteworthy that the N/C ratio is in the range of 0.032−0.043, suggesting that

388   NO_2 participated in the OH reaction of eugenol, through the addition to phenoxy

389   radical (Peng and Jimenez, 2017). Recently, Hunter et al. (2014) found that NO_2

390   participated in the OH reactions of cyclic alkanes, and the N/C ratios were in the range

391   of 0.031−0.064, higher than those obtained in this work. The nitro-substituted products

392   were reported to be the main reaction products of the OH reactions of guaiacol and

393   syringol in the presence of NO_2 (Lauraguais et al., 2014b; Ahmad et al., 2017). The N-

394   containing products might be also formed through the reactions involving with NO_3

395   radicals, which could be generated by the reaction between NO_2 and O_3 in this system

396   (Atkinson, 1991). Using the box model (Peng et al., 2015) and the maximum O_3

397   concentration (9.11 ppmv) in this work, the maximum NO_3 exposure was calculated to

398   be approximately 1.7×10^{11} molecules cm^{-3} s. Compared to the rate constant of eugenol

399   with OH radicals obtained in this work, the rate constant ($1.6 \times 10^{-13} cm^3$ molecule^{-1} s^{-}

400   ^{1}) of eugenol with NO_3 radicals was about 2 orders of magnitude lower (Zhang et al.,

401   2016). Thus, the contribution of NO_3 radicals on the decay of eugenol was insignificant.

402   The relative low volatility of N-containing products could reasonably contribute to SOA

403   formation (Duporté et al., 2016; Liu et al., 2016a). In addition, higher NO_2/NO ratio

404   favors the formation of nitro-substituted products, which are potentially involved in

405   NPF and SOA growth (Pereira et al., 2015). Ng et al. (2007a) also indicated that NO_x

406   could be beneficial to SOA formation for sesquiterpenes, due to the formation of low

407   volatility organic nitrates and the isomerization of large alkoxy radicals, resulting in

408   less volatile products. The decrease in the N/C ratio at high OH exposure suggested that

409   more volatile products were generated through the oxidation of particle-phase species

410   by OH radicals.

411   The NO^+ / NO_2^+ ratios measured by the HR-ToF-AMS are widely used to identify

412   inorganic and organic nitrates. The NO^+/NO_2^+ ratios for inorganic nitrates have been

413   reported to be in the range of 1.08−2.81 (Farmer et al., 2010; Sato et al., 2010). The

414   ratio ranged from 2.06 to 2.54 in this work as determined by the HR-ToF-AMS using

415   ammonium nitrate as the calibration sample. However, the NO^+/NO_2^+ ratios during

416   oxidation of eugenol in the presence of 40 ppbv NO_2 were 3.98−6.09. They were higher

417   than those for inorganic nitrates and consistent with those for organic nitrates

418   (3.82−5.84) from the photooxidation of aromatics (Sato et al., 2010). According to the

419   method described by Fry et al. (2013) (shown in Supplement), the fraction of organic

420   nitrate was calculated to be in the range of 25.64% to 82.05%, using the NO^+/NO_2^+

421   ratios (3.98−6.09) obtained at different OH exposure. The results were comparable to

422   those reported in earlier studies (Liu et al., 2015; Hunter et al., 2014). Liu et al. (2015)

423   reported that the N-containing organic mass contributed 31.5 ± 4.4% to the total SOA

424   derived from m-xylene oxidation by OH radicals. Hunter et al. (2014) estimated the

425   organic nitrate yields of SOA to be 31−64%, formed in the OH-initiated reactions of

426   acyclic, monocyclic, and polycyclic alkanes. This range obtained in this work should

427   be the upper limit due to the possibility of C−C bond scission of gas- and particle-phase

428   organics oxidized by high OH exposure. Besides, the maximum yield of nitrates for a

429   single reaction step is expected to be approximately 30% (Ziemann and Atkinson, 2012),

430   this suggests that multiple reaction steps are needed.

431   **3.5 Atmospheric implications**

432   Biomass burning not only serves as a major contributor of atmospheric primary organic

433   aerosol (POA), but also has great SOA formation potential through atmospheric

434   oxidation (Bruns et al., 2016; Gilardoni et al., 2016; Li et al., 2017; Ciarelli et al., 2017;

435   Ding et al., 2017). Recent studies have indicated that SOA formed from biomass

436   burning plays an important role in haze pollution in China (Li et al., 2017; Ding et al.,

437   2017). Residential combustion (mainly wood burning) could contribute approximately

438   60−70% to SOA formation in winter at the European scale (Ciarelli et al., 2017). In

439   addition, methoxyphenols are the major component of OA from biomass burning

440   (Bruns et al., 2016; Schauer and Cass, 2000). Based on our results and those of previous

441   studies (Sun et al., 2010; Lauraguais et al., 2012, 2014b; Ahmad et al., 2017; Yee et al.,

442   2013; Ofner et al., 2011), more attention should be paid to the SOA formation from the

443   OH oxidation of biomass burning emissions and its subsequent effect on haze evolution,

444   especially in China with nationwide biomass burning and high daytime average [OH]

445   in the ambient atmosphere (($5.2−7.5$) × 10^6 molecules cm^{-3}) (Yang et al., 2017).

446   Meanwhile, the potential contributions of SO_2 and NO_2 to SOA formation should also

447   be taken into account, because the concentrations of NO_x and SO_2 could be up to close

448   200 ppbv in the severely polluted atmosphere in China (Li et al., 2017). Although

449   eugenol concentrations in this work are higher than those in the ambient atmosphere,

450   the results obtained in this work could provide new information for SOA formation

451   from the atmospheric oxidation of methoxyphenols, and might be useful for SOA

452   modeling, especially for air quality simulation modeling of the specific regions

453   experiencing serious pollution caused by fine particulate matter.

454   N-containing products formed from the oxidation of methoxyphenols could

455   contribute to water-soluble organics in SOA (Lauraguais et al., 2014b; Yang et al., 2016;

456   Zhang et al., 2016), which have been widely detected in atmospheric humic-like

457   substances (HULIS) (Wang et al., 2017). Due to their surface-active and UV-light-

458   absorbing properties, HULIS could influence the formation of cloud condensation

459   nuclei (CCN), solar radiation balance, and photochemical processes in the atmosphere

460   (Wang et al., 2017). In addition, the formation of oligomers in particle phase via OH-

461   initiated reaction of methoxyphenols, which has been observed in aquesous oxidation

462   of phenolic species (Yu et al., 2014), might also enhance light absorption in UV-visible

463   region. The high reactivity of methoxyphenols toward atmospheric radicals suggests

464   that SOA was formed from their oxidation processes with relatively high oxidation level,

465   subsequently leading to SOA with strong optical absorption and hygroscopic properties

466   (Lambe et al., 2013; Massoli et al., 2010). Therefore, SOA formed from the reactions

467   of methoxyphenols with atmospheric oxidants might have important effects on air

468   quality and climate. In addition, the experimental results from this study would help to

469   further the understanding of the atmospheric aging process of smoke plumes from

470   biomass-burning emissions.

471   **4   Conclusions**

472   For the first time, the rate constant and SOA formation from the gas-phase reaction of

473   eugenol with OH radicals were investigated in an OFR. The second-order rate constant

474   of eugenol with OH radicals was $(8.01 \pm 0.40) \times 10^{-11}$ cm^3 molecule^{-1} s^{-1}, measured by

475 the relative rate method, and the corresponding atmospheric lifetime was (2.31 ± 0.12)

476 h. In addition, the significant SOA formation of eugenol oxidation by OH radicals was

477 observed. The maximum SOA yields $(0.11-0.31)$ obtained at different eugenol

478 concentrations could be expressed well by a one-product model. SOA yield was

479 dependent on OH exposure and eugenol concentration, which firstly increased and then

480 decreased as a function of OH exposure due to the possible C−C bond scission of gas-

481 phase species by further oxidation or heterogeneous reactions involving OH radicals.

482 The OS_C and O/C ratio both increased significantly as a function of OH exposure,

483 suggesting that SOA became more oxidized. The presence of SO_2 and NO_2 was helpful

484 to increase SOA yield, and the maximum enhanced yields were 38.6% and 19.2%,

485 respectively. The observed N/C ratio of SOA was in the range of $0.032-0.043$,

486 indicating that NO_2 participated in the OH-initiated reaction of eugenol, consequently

487 producing organic nitrates. The experimental results might be helpful to further

488 understand the atmospheric chemical behavior of eugenol and its SOA formation

489 potential from OH oxidation in the atmosphere.

490 **Data availability**

491 The experimental data are available upon request to the corresponding authors.

492 **Competing interests**

493 The authors declare that they have no conflict of interest.

494 **Author contributions**

495 C.L., Y.L., and H.H. designed the research and wrote the manuscript. C.L., T.C., and

496 J.L. performed the experiments. C.L., Y.L., T.C., J.L., and H.H. carried out the data

497 analysis. All authors contributed to the final manuscript.

507 **References**

508 Ahlberg, E., Falk, J., Eriksson, A., Holst, T., Brune, W. H., Kristensson, A., Roldin, P.,
509   and Svenningsson, B.: Secondary organic aerosol from VOC mixtures in an
510   oxidation flow reactor, Atmos. Environ., 161, 210-220, doi:
511   10.1016/j.atmosenv.2017.05.005, 2017.
512 Ahmad, W., Coeur, C., Tomas, A., Fagniez, T., Brubach, J.-B., and Cuisset, A.: Infrared
513   spectroscopy of secondary organic aerosol precursors and investigation of the
514   hygroscopicity of SOA formed from the OH reaction with guaiacol and syringol,
515   Appl. Opt., 56, E116-E122, doi: 10.1364/ao.56.00e116, 2017.
516 Atkinson, R., Perry, R. A., and Pitts, J. N.: Rate constants for the reactions of the OH
517   radicals with NO_2 (M = Ar and N_2) and SO_2 (M = Ar), J. Chem. Phys., 65, 306-
518   310, doi: 10.1063/1.432770, 1976.
519 Atkinson, R.: Kinetics and mechanisms of the gas-phase reactions of the NO_3 radical
520   with organic compounds, J. Phys. Chem. Ref. Data, 20, 459-507, doi:
521   10.1063/1.555887, 1991.

Atkinson, R., and Arey, J.: Atmospheric degradation of volatile organic compounds, Chem. Rev., 103, 4605-4638, doi: 10.1021/cr0206420, 2003.

Bari, M. A., Baumbach, G., Kuch, B., and Scheffknecht, G.: Wood smoke as a source of particle-phase organic compounds in residential areas, Atmos. Environ., 43, 4722-4732, doi: 10.1016/j.atmosenv.2008.09.006, 2009.

Bari, M. A., Baumbach, G., Kuch, B., and Scheffknecht, G.: Temporal variation and impact of wood smoke pollution on a residential area in southern Germany, Atmos. Environ., 44, 3823-3832, doi: 10.1016/j.atmosenv.2010.06.031, 2010.

Bolling, A. K., Pagels, J., Yttri, K. E., Barregard, L., Sallsten, G., Schwarze, P. E., and Boman, C.: Health effects of residential wood smoke particles: the importance of combustion conditions and physicochemical particle properties, Part. Fibre Toxicol., 6, doi: 10.1186/1743-8977-6-29, 2009.

Bruns, E. A., El Haddad, I., Keller, A., Klein, F., Kumar, N. K., Pieber, S. M., Corbin, J. C., Slowik, J. G., Brune, W. H., Baltensperger, U., and Prevot, A. S. H.: Inter-comparison of laboratory smog chamber and flow reactor systems on organic aerosol yield and composition, Atmos. Meas. Tech., 8, 2315-2332, doi: 10.5194/amt-8-2315-2015, 2015.

Bruns, E. A., El Haddad, I., Slowik, J. G., Kilic, D., Klein, F., Baltensperger, U., and Prevot, A. S. H.: Identification of significant precursor gases of secondary organic aerosols from residential wood combustion, Sci. Rep., 6., doi: 10.1038/srep27881, 2016.

Cao, G., and Jang, M.: Effects of particle acidity and UV light on secondary organic aerosol formation from oxidation of aromatics in the absence of NO_x, Atmos. Environ., 41, 7603-7613, doi: 10.1016/j.atmosenv.2007.05.034, 2007.

Chen, Y., and Bond, T. C.: Light absorption by organic carbon from wood combustion, Atmos. Chem. Phys., 10, 1773-1787, doi: 10.5194/acp-10-1773-2010, 2010.

Ciarelli, G., Aksoyoglu, S., El Haddad, I., Bruns, E. A., Crippa, M., Poulain, L., Aijala, M., Carbone, S., Freney, E., O'Dowd, C., Baltensperger, U., and Prevot, A. S. H.: Modelling winter organic aerosol at the European scale with CAMx: Evaluation and source apportionment with a VBS parameterization based on novel wood burning smog chamber experiments, Atmos. Chem. Phys., 7, 7653-7669, doi: 10.5194/acp-17-7653-2017, 2017.

Coeur-Tourneur, C., Cassez, A., and Wenger, J. C.: Rate Coefficients for the gas-phase reaction of hydroxyl radicals with 2-methoxyphenol (guaiacol) and related compounds, J. Phys. Chem. A, 114, 11645-11650, doi: 10.1021/jp1071023, 2010a.

Coeur-Tourneur, C., Foulon, V., and Lareal, M.: Determination of aerosol yields from 3-methylcatechol and 4-methylcatechol ozonolysis in a simulation chamber, Atmos. Environ., 44, 852-857, doi: 10.1016/j.atmosenv.2009.11.027, 2010b.

Davis, D. D., Ravishankara, A. R., and Fischer, S.: SO_2 oxidation via the hydroxyl radical: Atmospheric fate of HSO_x radicals, Geophys. Res. Lett., 6, 113-116, doi: 10.1029/GL006i002p00113, 1979.

DeCarlo, P. F., Slowik, J. G., Worsnop, D. R., Davidovits, P., and Jimenez, J. L.: Particle

564 morphology and density characterization by combined mobility and aerodynamic
565 diameter measurements. Part 1: Theory, Aerosol Sci. Technol., 38, 1185-1205, doi:
566 10.1080/027868290903907, 2004.

567 DeCarlo, P. F., Kimmel, J. R., Trimborn, A., Northway, M. J., Jayne, J. T., Aiken, A. C.,
568 Gonin, M., Fuhrer, K., Horvath, T., Docherty, K. S., Worsnop, D. R., and Jimenez,
569 J. L.: Field-deployable, high-resolution, time-of-flight aerosol mass spectrometer,
570 Anal. Chem., 78, 8281-8289, doi: 10.1021/ac061249n, 2006.

571 Dills, R. L., Paulsen, M., Ahmad, J., Kalman, D. A., Elias, F. N., and Simpson, C. D.:
572 Evaluation of urinary methoxyphenols as biomarkers of woodsmoke exposure,
573 Environ. Sci. Technol., 40, 2163-2170, doi: 10.1021/es051886f, 2006.

574 Ding, X., Zhang, Y.-Q., He, Q.-F., Yu, Q.-Q., Wang, J.-Q., Shen, R.-Q., Song, W., Wang,
575 Y.-S., and Wang, X.-M.: Significant increase of aromatics-derived secondary
576 organic aerosol during fall to winter in China, Environ. Sci. Technol., 51, 7432-
577 7441, doi: 10.1021/acs.est.6b06408, 2017.

578 Duporté, G., Parshintsev, J., Barreira, L. M. F., Hartonen, K., Kulmala, M., and
579 Riekkola, M.-L.: Nitrogen-containing low volatile compounds from
580 pinonaldehyde-dimethylamine reaction in the atmosphere: A laboratory and field
581 study, Environ. Sci. Technol., 50, 4693-4700, doi: 10.1021/acs.est.6b00270, 2016.

582 El Zein, A., Coeur, C., Obeid, E., Lauraguais, A., and Fagniez, T.: Reaction kinetics of
583 catechol (1,2-benzenediol) and guaiacol (2-methoxyphenol) with ozone, J. Phys.
584 Chem. A, 119, 6759-6765, doi: 10.1021/acs.jpca.5b00174, 2015.

585 Farmer, D. K., Matsunaga, A., Docherty, K. S., Surratt, J. D., Seinfeld, J. H., Ziemann,
586 P. J., and Jimenez, J. L.: Response of an aerosol mass spectrometer to
587 organonitrates and organosulfates and implications for atmospheric chemistry,
588 Proc. Natl. Acad. Sci. U. S. A, 107, 6670-6675, doi: 10.1073/pnas.0912340107,
589 2010.

590 Finewax, Z., de Gouw, J. A., and Ziemann, P. J.: Identification and quantification of 4-
591 nitrocatechol formed from OH and NO_3 radical-initiated reactions of catechol in
592 air in the presence of NO_x: Implications for secondary organic aerosol formation
593 from biomass burning, Environ. Sci. Technol., 52, 1981-1989, doi:
594 10.1021/acs.est.7b05864, 2018.

595 Friedman, B., Brophy, P., Brune, W. H., and Farmer, D. K.: Anthropogenic sulfur
596 perturbations on biogenic oxidation: SO_2 additions impact gas-phase OH oxidation
597 products of alpha- and beta-pinene, Environ. Sci. Technol., 50, 1269-1279, doi:
598 10.1021/acs.est.5b05010, 2016.

599 Fry, J. L., Draper, D. C., Zarzana, K. J., Campuzano-Jost, P., Day, D. A., Jimenez, J. L.,
600 Brown, S. S., Cohen, R. C., Kaser, L., Hansel, A., Cappellin, L., Karl, T., Hodzic
601 Roux, A., Turnipseed, A., Cantrell, C., Lefer, B. L., and Grossberg, N.:
602 Observations of gas- and aerosol-phase organic nitrates at BEACHON-RoMBAS
603 2011, Atmos. Chem. Phys., 13, 8585-8605, 10.5194/acp-13-8585-2013, 2013.

604 Gilardoni, S., Massoli, P., Paglione, M., Giulianelli, L., Carbone, C., Rinaldi, M.,
605 Decesari, S., Sandrini, S., Costabile, F., Gobbi, G. P., Pietrogrande, M. C., Visentin,

606   M., Scotto, F., Fuzzi, S., and Facchini, M. C.: Direct observation of aqueous
607   secondary organic aerosol from biomass-burning emissions, Proc. Natl. Acad. Sci.
608   U. S. A, 113, 10013-10018, doi: 10.1073/pnas.1602212113, 2016.

609 Gordon, T. D., Presto, A. A., Nguyen, N. T., Robertson, W. H., Na, K., Sahay, K. N.,
610   Zhang, M., Maddox, C., Rieger, P., Chattopadhyay, S., Maldonado, H., Maricq, M.
611   M., and Robinson, A. L.: Secondary organic aerosol production from diesel
612   vehicle exhaust: impact of aftertreatment, fuel chemistry and driving cycle, Atmos.
613   Chem. Phys., 14, 4643-4659, doi: 10.5194/acp-14-4643-2014, 2014.

614 http://www.aim.env.uea.ac.uk/aim/model2/model2a.php.

615 Hunter, J. F., Carrasquillo, A. J., Daumit, K. E., and Kroll, J. H.: Secondary organic
616   aerosol formation from acyclic, monocyclic, and polycyclic alkanes, Environ. Sci.
617   Technol., 48, 10227-10234, doi: 10.1021/es502674s, 2014.

618 Jaoui, M., Edney, E. O., Kleindienst, T. E., Lewandowski, M., Offenberg, J. H., Surratt,
619   J. D., and Seinfeld, J. H.: Formation of secondary organic aerosol from irradiated
620   alpha-pinene/toluene/NO_x mixtures and the effect of isoprene and sulfur dioxide,
621   J. Geophys. Res.-Atmos., 113, doi: 10.1029/2007jd009426, 2008.

622 Jeong, C.-H., Evans, G. J., Dann, T., Graham, M., Herod, D., Dabek-Zlotorzynska, E.,
623   Mathieu, D., Ding, L., and Wang, D.: Influence of biomass burning on wintertime
624   fine particulate matter: Source contribution at a valley site in rural British
625   Columbia, Atmos. Environ., 42, 3684-3699, doi: 10.1016/j.atmosenv.2008.01.006,
626   2008.

627 Kang, E., Root, M. J., Toohey, D. W., and Brune, W. H.: Introducing the concept of
628   Potential Aerosol Mass (PAM), Atmos. Chem. Phys., 7, 5727-5744, doi:
629   10.5194/acp-7-5727-2007, 2007.

630 Keck, L., and Wittmaack, K.: Effect of filter type and temperature on volatilisation
631   losses from ammonium salts in aerosol matter, Atmos. Environ., 39, 4093-4100,
632   doi: 10.1016/j.atmosenv.2005.03.029, 2005.

633 Kleindienst, T. E., Shepson, P. B., Edney, E. O., Claxton, L. D., and Cupitt, L. T.: Wood
634   smoke: Measurement of the mutagenic activities of its gas- and particulate-phase
635   photooxidation products, Environ. Sci. Technol., 20, 493-501, doi:
636   10.1021/es00147a009, 1986.

637 Kleindienst, T. E., Edney, E. O., Lewandowski, M., Offenberg, J. H., and Jaoui, M.:
638   Secondary organic carbon and aerosol yields from the irradiations of isoprene and
639   alpha-pinene in the presence of NO_x and SO_2, Environ. Sci. Technol., 40, 3807-
640   3812, doi: 10.1021/es052446r, 2006.

641 Kramp, F., and Paulson, S. E.: On the uncertainties in the rate coefficients for OH
642   reactions with hydrocarbons, and the rate coefficients of the 1,3,5-
643   trimethylbenzene and m-xylene reactions with OH radicals in the gas phase, J.
644   Phys. Chem. A, 102, 2685-2690, doi: 10.1021/jp973289o, 1998.

645 Kroll, J. H., Donahue, N. M., Jimenez, J. L., Kessler, S. H., Canagaratna, M. R., Wilson,
646   K. R., Altieri, K. E., Mazzoleni, L. R., Wozniak, A. S., Bluhm, H., Mysak, E. R.,
647   Smith, J. D., Kolb, C. E., and Worsnop, D. R.: Carbon oxidation state as a metric

648 for describing the chemistry of atmospheric organic aerosol, Nature Chem., 3, 133-
649 139, doi: 10.1038/nchem.948, 2011.

650 Lambe, A. T., Cappa, C. D., Massoli, P., Onasch, T. B., Forestieri, S. D., Martin, A. T.,
651 Cummings, M. J., Croasdale, D. R., Brune, W. H., Worsnop, D. R., and Davidovits,
652 P.: Relationship between oxidation level and optical properties of secondary
653 organic aerosol, Environ. Sci. Technol., 47, 6349-6357, doi: 10.1021/es401043j,
654 2013.

655 Lambe, A. T., Chhabra, P. S., Onasch, T. B., Brune, W. H., Hunter, J. F., Kroll, J. H.,
656 Cummings, M. J., Brogan, J. F., Parmar, Y., Worsnop, D. R., Kolb, C. E., and
657 Davidovits, P.: Effect of oxidant concentration, exposure time, and seed particles
658 on secondary organic aerosol chemical composition and yield, Atmos. Chem.
659 Phys., 15, 3063-3075, doi: 10.5194/acp-15-3063-2015, 2015.

660 Lauraguais, A., Coeur-Tourneur, C., Cassez, A., and Seydi, A.: Rate constant and
661 secondary organic aerosol yields for the gas-phase reaction of hydroxyl radicals
662 with syringol (2,6-dimethoxyphenol), Atmos. Environ., 55, 43-48, doi:
663 10.1016/j.atmosenv.2012.02.027, 2012.

664 Lauraguais, A., Bejan, I., Barnes, I., Wiesen, P., Coeur-Tourneur, C., and Cassez, A.:
665 Rate coefficients for the gas-phase reaction of chlorine atoms with a series of
666 methoxylated aromatic compounds, J. Phys. Chem. A, 118, 1777-1784, doi:
667 10.1021/jp4114877, 2014a.

668 Lauraguais, A., Coeur-Tourneur, C., Cassez, A., Deboudt, K., Fourmentin, M., and
669 Choel, M.: Atmospheric reactivity of hydroxyl radicals with guaiacol (2-
670 methoxyphenol), a biomass burning emitted compound: Secondary organic
671 aerosol formation and gas-phase oxidation products, Atmos. Environ., 86, 155-163,
672 doi: 10.1016/j.atmosenv.2013.11.074, 2014b.

673 Lauraguais, A., Bejan, I., Barnes, I., Wiesen, P., and Coeur, C.: Rate coefficients for the
674 gas-phase reactions of hydroxyl radicals with a series of methoxylated aromatic
675 compounds, J. Phys. Chem. A, 119, 6179-6187, doi: 10.1021/acs.jpca.5b03232,
676 2015.

677 Lauraguais, A., El Zein, A., Coeur, C., Obeid, E., Cassez, A., Rayez, M.-T., and Rayez,
678 J.-C.: Kinetic study of the gas-phase reactions of nitrate radicals with
679 methoxyphenol compounds: Experimental and theoretical approaches, J. Phys.
680 Chem. A, 120, 2691-2699, doi: 10.1021/acs.jpca.6b02729, 2016.

681 Li, H., Zhang, Q., Zhang, Q., Chen, C., Wang, L., Wei, Z., Zhou, S., Parworth, C., Zheng,
682 B., Canonaco, F., Prevot, A. S. H., Chen, P., Zhang, H., Wallington, T. J., and He,
683 K.: Wintertime aerosol chemistry and haze evolution in an extremely polluted city
684 of the North China Plain: Significant contribution from coal and biomass
685 combustion, Atmos. Chem. Phys., 17, 4751-4768, doi: 10.5194/acp-17-4751-2017,
686 2017.

687 Li, R., Palm, B. B., Ortega, A. M., Hlywiak, J., Hu, W., Peng, Z., Day, D. A., Knote, C.,
688 Brune, W. H., de Gouw, J. A., and Jimenez, J. L.: Modeling the radical chemistry
689 in an oxidation flow reactor: Radical formation and recycling, sensitivities, and

the OH exposure estimation equation, J. Phys. Chem. A, 119, 4418-4432, doi: 10.1021/jp509534k, 2015.

Liu, J., Lin, P., Laskin, A., Laskin, J., Kathmann, S. M., Wise, M., Caylor, R., Imholt, F., Selimovic, V., and Shilling, J. E.: Optical properties and aging of light-absorbing secondary organic aerosol, Atmos. Chem. Phys., 16, 12815-12827, doi: 10.5194/acp-16-12815-2016, 2016a.

Liu, T., Wang, X., Hu, Q., Deng, W., Zhang, Y., Ding, X., Fu, X., Bernard, F., Zhang, Z., Lu, S., He, Q., Bi, X., Chen, J., Sun, Y., Yu, J., Peng, P., Sheng, G., and Fu, J.: Formation of secondary aerosols from gasoline vehicle exhaust when mixing with SO_2, Atmos. Chem. Phys., 16, 675-689, doi: 10.5194/acp-16-675-2016, 2016b.

Liu, Y., Huang, L., Li, S. M., Harner, T., and Liggio, J.: OH-initiated heterogeneous oxidation of tris-2-butoxyethyl phosphate: implications for its fate in the atmosphere, Atmos. Chem. Phys., 14, 12195-12207, 10.5194/acp-14-12195-2014, 2014a.

Liu, Y., Liggio, J., Harner, T., Jantunen, L., Shoeib, M., and Li, S.-M.: Heterogeneous OH initiated oxidation: A possible explanation for the persistence of organophosphate flame retardants in air, Environ. Sci. Technol., 48, 1041-1048, doi: 10.1021/es404515k, 2014b.

Liu, Y., Liggio, J., Staebler, R., and Li, S. M.: Reactive uptake of ammonia to secondary organic aerosols: Kinetics of organonitrogen formation, Atmos. Chem. Phys., 15, 13569-13584, doi: 10.5194/acp-15-13569-2015, 2015.

Mao, J., Ren, X., Brune, W. H., Olson, J. R., Crawford, J. H., Fried, A., Huey, L. G., Cohen, R. C., Heikes, B., Singh, H. B., Blake, D. R., Sachse, G. W., Diskin, G. S., Hall, S. R., and Shetter, R. E.: Airborne measurement of OH reactivity during INTEX-B, Atmos. Chem. Phys., 9, 163-173, doi: 10.5194/acp-9-163-2009, 2009.

Massoli, P., Lambe, A. T., Ahern, A. T., Williams, L. R., Ehn, M., Mikkila, J., Canagaratna, M. R., Brune, W. H., Onasch, T. B., Jayne, J. T., Petaja, T., Kulmala, M., Laaksonen, A., Kolb, C. E., Davidovits, P., and Worsnop, D. R.: Relationship between aerosol oxidation level and hygroscopic properties of laboratory generated secondary organic aerosol (SOA) particles, Geophys. Res. Lett., 37, doi: 10.1029/2010gl045258, 2010.

McMurry, J. E.: Organic Chemistry, 6th ed., 2004.

Ng, N. L., Chhabra, P. S., Chan, A. W. H., Surratt, J. D., Kroll, J. H., Kwan, A. J., McCabe, D. C., Wennberg, P. O., Sorooshian, A., Murphy, S. M., Dalleska, N. F., Flagan, R. C., and Seinfeld, J. H.: Effect of NOx level on secondary organic aerosol (SOA) formation from the photooxidation of terpenes, Atmos. Chem. Phys., 7, 5159-5174, doi: 10.5194/acp-7-5159-2007, 2007a.

Ng, N. L., Kroll, J. H., Chan, A. W. H., Chhabra, P. S., Flagan, R. C., and Seinfeld, J. H.: Secondary organic aerosol formation from m-xylene, toluene, and benzene, Atmos. Chem. Phys., 7, 3909-3922, doi: 10.5194/acp-7-3909-2007, 2007b.

Ng, N. L., Canagaratna, M. R., Zhang, Q., Jimenez, J. L., Tian, J., Ulbrich, I. M., Kroll, J. H., Docherty, K. S., Chhabra, P. S., Bahreini, R., Murphy, S. M., Seinfeld, J. H.,

Hildebrandt, L., Donahue, N. M., DeCarlo, P. F., Lanz, V. A., Prevot, A. S. H., Dinar, E., Rudich, Y., and Worsnop, D. R.: Organic aerosol components observed in Northern Hemispheric datasets from Aerosol Mass Spectrometry, Atmos. Chem. Phys., 10, 4625-4641, doi: 10.5194/acp-10-4625-2010, 2010.

Nolte, C. G., Schauer, J. J., Cass, G. R., and Simoneit, B. R. T.: Highly polar organic compounds present in wood smoke and in the ambient atmosphere, Environ. Sci. Technol., 35, 1912-1919, doi: 10.1021/es001420r, 2001.

Odum, J. R., Hoffmann, T., Bowman, F., Collins, D., Flagan, R. C., and Seinfeld, J. H.: Gas/particle partitioning and secondary organic aerosol yields, Environ. Sci. Technol., 30, 2580-2585, doi: 10.1021/es950943+, 1996.

Ofner, J., Krueger, H. U., Grothe, H., Schmitt-Kopplin, P., Whitmore, K., and Zetzsch, C.: Physico-chemical characterization of SOA derived from catechol and guaiacol - a model substance for the aromatic fraction of atmospheric HULIS, Atmos. Chem. Phys., 11, 1-15, doi: 10.5194/acp-11-1-2011, 2011.

Ortega, A. M., Hayes, P. L., Peng, Z., Palm, B. B., Hu, W., Day, D. A., Li, R., Cubison, M. J., Brune, W. H., Graus, M., Warneke, C., Gilman, J. B., Kuster, W. C., de Gouw, J., Gutierrez-Montes, C., and Jimenez, J. L.: Real-time measurements of secondary organic aerosol formation and aging from ambient air in an oxidation flow reactor in the Los Angeles area, Atmos. Chem. Phys., 16, 7411-7433, doi: 10.5194/acp-16-7411-2016, 2016.

Palm, B. B., Campuzano-Jost, P., Ortega, A. M., Day, D. A., Kaser, L., Jud, W., Karl, T., Hansel, A., Hunter, J. F., Cross, E. S., Kroll, J. H., Peng, Z., Brune, W. H., and Jimenez, J. L.: In situ secondary organic aerosol formation from ambient pine forest air using an oxidation flow reactor, Atmos. Chem. Phys., 16, 2943-2970, 10.5194/acp-16-2943-2016, 2016.

Palm, B. B., de Sá, S. S., Day, D. A., Campuzano-Jost, P., Hu, W., Seco, R., Sjostedt, S. J., Park, J. H., Guenther, A. B., Kim, S., Brito, J., Wurm, F., Artaxo, P., Thalman, R., Wang, J., Yee, L. D., Wernis, R., Isaacman-VanWertz, G., Goldstein, A. H., Liu, Y., Springston, S. R., Souza, R., Newburn, M. K., Alexander, M. L., Martin, S. T., and Jimenez, J. L.: Secondary organic aerosol formation from ambient air in an oxidation flow reactor in central Amazonia, Atmos. Chem. Phys., 18, 467-493, 10.5194/acp-18-467-2018, 2018.

Peng, Z., Day, D. A., Stark, H., Li, R., Lee-Taylor, J., Palm, B. B., Brune, W. H., and Jimenez, J. L.: HOx radical chemistry in oxidation flow reactors with low-pressure mercury lamps systematically examined by modeling, Atmos. Meas. Tech., 8, 4863-4890, doi: 10.5194/amt-8-4863-2015, 2015.

Peng, Z., Day, D. A., Ortega, A. M., Palm, B. B., Hu, W., Stark, H., Li, R., Tsigaridis, K., Brune, W. H., and Jimenez, J. L.: Non-OH chemistry in oxidation flow reactors for the study of atmospheric chemistry systematically examined by modeling, Atmos. Chem. Phys., 16, 4283-4305, doi: 10.5194/acp-16-4283-2016, 2016.

Peng, Z., and Jimenez, J. L.: Modeling of the chemistry in oxidation flow reactors with high initial NO, Atmos. Chem. Phys., 17, 11991-12010, doi: 10.5194/acp-17-

774   11991-2017, 2017.

775 Pereira, K. L., Hamilton, J. F., Rickard, A. R., Bloss, W. J., Alam, M. S., Camredon, M.,
776   Ward, M. W., Wyche, K. P., Munoz, A., Vera, T., Vazquez, M., Borras, E., and
777   Rodenas, M.: Insights into the formation and evolution of individual compounds
778   in the particulate phase during aromatic photo-oxidation, Environ. Sci. Technol.,
779   49, 13168-13178, doi: 10.1021/acs.est.5b03377, 2015.

780 Priya, A. M., and Lakshmipathi, S.: DFT study on abstraction reaction mechanism of
781   oh radical with 2-methoxyphenol, J. Phys. Org. Chem., 30, e3713,
782   doi:10.1002/poc.3713, 2017.

783 Sarrafzadeh, M., Wildt, J., Pullinen, I., Springer, M., Kleist, E., Tillmann, R., Schmitt,
784   S. H., Wu, C., Mentel, T. F., Zhao, D., Hastie, D. R., and Kiendler-Scharr, A.:
785   Impact of NOx and OH on secondary organic aerosol formation from beta-pinene
786   photooxidation, Atmos. Chem. Phys., 16, 11237-11248, doi: 10.5194/acp-16-
787   11237-2016, 2016.

788 Sato, K., Takami, A., Isozaki, T., Hikida, T., Shimono, A., and Imamura, T.: Mass
789   spectrometric study of secondary organic aerosol formed from the photo-oxidation
790   of aromatic hydrocarbons, Atmos. Environ., 44, 1080-1087, doi:
791   10.1016/j.atmosenv.2009.12.013, 2010.

792 Schauer, J. J., and Cass, G. R.: Source apportionment of wintertime gas-phase and
793   particle-phase air pollutants using organic compounds as tracers, Environ. Sci.
794   Technol., 34, 1821-1832, doi: 10.1021/es981312t, 2000.

795 Schauer, J. J., Kleeman, M. J., Cass, G. R., and Simoneit, B. R. T.: Measurement of
796   emissions from air pollution sources. 3. C-1-C-29 organic compounds from
797   fireplace combustion of wood, Environ. Sci. Technol., 35, 1716-1728, doi:
798   10.1021/es001331e, 2001.

799 Simonen, P., Saukko, E., Karjalainen, P., Timonen, H., Bloss, M., Aakko-Saksa, P.,
800   Ronkko, T., Keskinen, J., and Dal Maso, M.: A new oxidation flow reactor for
801   measuring secondary aerosol formation of rapidly changing emission sources,
802   Atmos. Meas. Tech., 10, 1519-1537, doi: 10.5194/amt-10-1519-2017, 2017.

803 Simpson, C. D., Paulsen, M., Dills, R. L., Liu, L. J. S., and Kalman, D. A.:
804   Determination of methoxyphenols in ambient atmospheric particulate matter:
805   Tracers for wood combustion, Environ. Sci. Technol., 39, 631-637, doi:
806   10.1021/es0486871, 2005.

807 Sun, Y. L., Zhang, Q., Anastasio, C., and Sun, J.: Insights into secondary organic aerosol
808   formed via aqueous-phase reactions of phenolic compounds based on high
809   resolution mass spectrometry, Atmos. Chem. Phys., 10, 4809-4822, doi:
810   10.5194/acp-10-4809-2010, 2010.

811 Thuner, L. P., Bardini, P., Rea, G. J., and Wenger, J. C.: Kinetics of the gas-phase
812   reactions of OH and NO3 radicals with dimethylphenols, J. Phys. Chem. A, 108,
813   11019-11025, 10.1021/jp046358p, 2004.

814 Tiitta, P., Leskinen, A., Hao, L., Yli-Pirila, P., Kortelainen, M., Grigonyte, J., Tissari, J.,
815   Lamberg, H., Hartikainen, A., Kuuspalo, K., Kortelainen, A.-M., Virtanen, A.,

816   Lehtinen, K. E. J., Komppula, M., Pieber, S., Prevot, A. S. H., Onasch, T. B.,
817   Worsnop, D. R., Czech, H., Zimmermann, R., Jokiniemi, J., and Sippula, O.:
818   Transformation of logwood combustion emissions in a smog chamber: formation
819   of secondary organic aerosol and changes in the primary organic aerosol upon
820   daytime and nighttime aging, Atmos. Chem. Phys., 16, 13251-13269, doi:
821   10.5194/acp-16-13251-2016, 2016.

822 US EPA: Estimation Programs Interface Suite™ for Microsoft® Windows, v 4.11,
823   United States Environmental Protection Agency, Washington, DC, USA, 2012.

824 Wang, D., Zhou, B., Fu, Q., Zhao, Q., Zhang, Q., Chen, J., Yang, X., Duan, Y., and Li,
825   J.: Intense secondary aerosol formation due to strong atmospheric photochemical
826   reactions in summer: observations at a rural site in eastern Yangtze River Delta of
827   China, Sci. Total Environ., 571, 1454-1466, doi: 10.1016/j.scitotenv.2016.06.212,
828   2016.

829 Wang, Y., Hu, M., Lin, P., Guo, Q., Wu, Z., Li, M., Zeng, L., Song, Y., Zeng, L., Wu,
830   Y., Guo, S., Huang, X., and He, L.: Molecular characterization of nitrogen-
831   containing organic compounds in humic-like substances emitted from straw
832   residue burning, Environ. Sci. Technol., 51, 5951-5961, doi:
833   10.1021/acs.est7b00248, 2017.

834 Ward, T. J., Rinehart, L. R., and Lange, T.: The 2003/2004 Libby, Montana PM2.5
835   source apportionment research study, Aerosol Sci. Technol., 40, 166-177, doi:
836   10.1080/02786820500494536, 2006.

837 Xu, L., Middlebrook, A. M., Liao, J., de Gouw, J. A., Guo, H., Weber, R. J., Nenes, A.,
838   Lopez-Hilfiker, F. D., Lee, B. H., Thornton, J. A., Brock, C. A., Neuman, J. A.,
839   Nowak, J. B., Pollack, I. B., Welti, A., Graus, M., Warneke, C., and Ng, N. L.:
840   Enhanced formation of isoprene-derived organic aerosol in sulfur-rich power plant
841   plumes during Southeast Nexus, J. Geophys. Res.-Atmos., 121, 11137-11153, doi:
842   10.1002/2016jd025156, 2016.

843 Yang, B., Zhang, H., Wang, Y., Zhang, P., Shu, J., Sun, W., and Ma, P.: Experimental
844   and theoretical studies on gas-phase reactions of NO_3 radicals with three
845   methoxyphenols: Guaiacol, creosol, and syringol, Atmos. Environ., 125, 243-251,
846   doi: 10.1016/j.atmosenv.2015.11.028, 2016.

847 Yang, Y., Shao, M., Kessel, S., Li, Y., Lu, K., Lu, S., Williams, J., Zhang, Y., Zeng, L.,
848   Noelscher, A. C., Wu, Y., Wang, X., and Zheng, J.: How the OH reactivity affects
849   the ozone production efficiency: case studies in Beijing and Heshan, China, Atmos.
850   Chem. Phys., 17, 7127-7142, doi: 10.5194/acp-17-7127-2017, 2017.

851 Yee, L. D., Kautzman, K. E., Loza, C. L., Schilling, K. A., Coggon, M. M., Chhabra, P.
852   S., Chan, M. N., Chan, A. W. H., Hersey, S. P., Crounse, J. D., Wennberg, P. O.,
853   Flagan, R. C., and Seinfeld, J. H.: Secondary organic aerosol formation from
854   biomass burning intermediates: phenol and methoxyphenols, Atmos. Chem. Phys.,
855   13, 8019-8043, doi: 10.5194/acp-13-8019-2013, 2013.

856 Yu, L., Smith, J., Laskin, A., Anastasio, C., Laskin, J., and Zhang, Q.: Chemical
857   characterization of SOA formed from aqueous-phase reactions of phenols with the
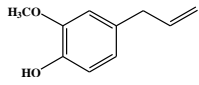
858   triplet excited state of carbonyl and hydroxyl radical, Atmos. Chem. Phys., 14,
859   13801-13816, 10.5194/acp-14-13801-2014, 2014.

860   Zhang, H., Yang, B., Wang, Y., Shu, J., Zhang, P., Ma, P., and Li, Z.: Gas-phase reactions
861   of methoxyphenols with NO_3 radicals: Kinetics, products, and mechanisms, J.
862   Phys. Chem. A, 120, 1213-1221, doi: 10.1021/acs.jpca.5b10406, 2016.

863   Zhang, X., Lambe, A. T., Upshur, M. A., Brooks, W. A., Be, A. G., Thomson, R. J.,
864   Geiger, F. M., Surratt, J. D., Zhang, Z., Gold, A., Graf, S., Cubison, M. J., Groessl,
865   M., Jayne, J. T., Worsnop, D. R., and Canagaratna, M. R.: Highly oxygenated
866   multifunctional compounds in alpha-pinene secondary organic aerosol, Environ.
867   Sci. Technol., 51, 5932-5940, doi: 10.1021/acs.est.6b06588, 2017.

868   Ziemann, P. J., and Atkinson, R.: Kinetics, products, and mechanisms of secondary
869   organic aerosol formation, Chem. Soc. Rev., 41, 6582-6605, doi:
870   10.1039/c2cs35122f, 2012.

Table 1. Rate constant for gas-phase reaction of eugenol with OH radicals and associated atmospheric lifetime.

Compound	Structure	References	k_E/k_R	k_E[a]	k_{OH}[a]	k_E (average)[a]	τ_{OH} (h)[b]
eugenol ($C_{10}H_{12}O_2$)		1,3,5-trimethylbeneze	1.33 ± 0.05	7.54 ± 0.28	6.50[c]	8.01 ± 0.40	2.31 ± 0.12
		m-xylene	3.85 ± 0.23	8.47 ± 0.51			

[a] Units of 10^{-11} cm^3 molecule^{-1} s^{-1}.

[b] Atmospheric lifetime in hours. $\tau_{OH}=1/k_E[OH]$, assuming a 24 h average $[OH] = 1.5 \times 10^6$ molecules cm^{-3} (Mao et al., 2009).

[c] Calculated using US EPA AOP WIN model (US EPA, 2012).

877   **Table 2.** Experimental conditions and results for SOA formation.

Expt.	[eugenol]$_0$[a]	△[eugenol][b]	M_o[c]	SO$_2$	NO$_2$	Y_{max}[d]	OH Exposure (10^{11} molecules cm^{-3} s)[e]	τ (d)[f]
	(μg m^{-3})	(μg m^{-3})	(μg m^{-3})	(ppbv)	(ppbv)			
#1	272	265	29	–	–	0.11	5.41	4.17
#2	351	339	54	–	–	0.16	5.41	4.17
#3	485	474	83	–	–	0.18	5.41	4.17
#4	636	625	145	–	–	0.23	5.41	4.17
#5	874	858	241	–	–	0.28	7.37	5.68
#6	1327	1304	399	–	–	0.31	8.91	6.87
#7	273	267	40	41	–	0.15	5.41	4.17
#8	273	266	35	–	40	0.13	5.41	4.17

878   [a] Initial eugenol concentrations.

879   [b] Reacted eugenol concentrations.

880   [c] SOA concentrations.

881   [d] Maximum SOA yields.

882   [e] Corresponding OH exposure of maximum SOA yields.

883   [f] Corresponding atmospheric aging time of maximum SOA yields, calculated using a

884   typical [OH] in the atmosphere in this work (1.5×10^6 molecules cm^{-3}) (Mao et al.,

885   2009).

886 **Figure Captions**

887 **Figure 1.** Relative rate plots for gas-phase reaction of OH radicals with eugenol.

888 **Figure 2.** Maximum SOA yields as a function of SOA mass concentration (M_o) formed

889 from the OH reactions at different eugenol concentrations. The solid line was fit to the

890 experimental data using a one-product model. Values for α_i and $K_{om,i}$ used to generate

891 the solid line are (0.36 ± 0.02) and (0.013 ± 0.002), respectively.

892 **Figure 3.** OS_C, H/C, and O/C vs. the OH exposure for SOA formed at two eugenol

893 concentrations (272 and 1328 $\mu g\ m^{-3}$).

894 **Figure 4.** Evolution of the enhanced SOA yield and sulfate formation as a function of

895 OH exposure in the presence of 41 ppbv SO_2 at average eugenol concentration of 273

896 $\mu g\ m^{-3}$.

897 **Figure 5.** Evolution of the enhanced SOA yields, nitrate formation, and N/C ratio as a

898 function of OH exposure in the presence of 40 ppbv NO_2 at average eugenol

899 concentration of 273 $\mu g\ m^{-3}$.